ANNALS OF GEOPHYSICS, 67, 5, S548, 2024; doi:10.4401/ag-9106
OPEN ACCESS

Analysis of stress changes on the Poso fault caused by large inland earthquakes: Case study of the 2017 Mw 6.6 Poso and the 2018 Mw 7.5 Palu-Donggala earthquakes

Muh. Altin Massinai[1], Muhammad Taufiq Rafie[*,1], Tsaqif Razin[2], M. Alimuddin Hamzah Assagaf[3], Erfan Syamsuddin[1], Maria Maria[1]

(1) Hasanuddin University, Solid Geophysics Laboratory, Department of Geophysics, Faculty of Mathematics and Natural Sciences, Makassar, Indonesia
(2) Hasanuddin University, Program Study of Geophysics, Department of Geophysics, Faculty of Mathematics and Natural Sciences, Makassar, Indonesia
(3) Hasanuddin University, Coastal and Ocean Dynamics Laboratory, Department of Geophysics, Faculty of Mathematics and Natural Sciences, Makassar, Indonesia

Article history: received April 24, 2024; accepted August 31, 2024

Abstract

The 2017 Mw 6.6 Poso and the 2018 Mw 7.5 Palu-Donggala represent significant seismic events in central Sulawesi Island. These events transferred the stress to the surrounding faults, which can promote or inhibit the critical condition in a fault, thus evaluating the stress transfer from these earthquakes is crucial for a comprehensive understanding of fault behaviour. In this study, we investigate the effect of these large events by resolving the accumulated Coulomb stress change onto a multi-strike segment of the Poso fault. Additionally, we also used GPS measurement (Global Strain Rate Model) to estimate the increase in tectonic stress rate due to coupling of triple-junction plate convergence. The 2017 Poso earthquake induces positive stress changes (7 kPa to 27 kPa) in the central segment, negative changes (−4 kPa to −10 kPa) in the northern segment, and less significant effects in the southern segment. The 2018 Palu-Donggala earthquake imparts a notably high negative Coulomb stress (−16 kPa to −27 kPa) across the entire northern segment. Cumulatively, both earthquakes reduce Coulomb stress predominantly in the northern part of the Poso fault, suggesting a delayed critical point. Furthermore, the analysis of the Coulomb stress changes time function indicates that stress accumulation in the northern Poso fault is more modulated by large earthquakes, while stress accumulation in the southern segments may be more controlled by long-term tectonic stress loading. The stress accumulation model developed in this study can provide a guidance in better understanding further earthquake risk mitigation in central Sulawesi.

Keywords: Coulomb stress changes; Sulawesi Island; Poso fault; Large inland earthquakes

1. Introduction

Sulawesi Island has one of the most intricate tectonic settings, characterized by the convergence of three major plates: The Philippine Sea, Indo-Australian, and Sunda Plates, forming a triple-junction convergence zone. The convergence process between the Philippine Sea and Indo-Australian Plates relative to Sunda Plate is facilitated by subduction in the north and block rotation of the Molucca Sea, Banda Sea and Timor Plate. Consequently, the island hosts numerous active faults (Bellier et al., 2006; Vigny et al., 2002; Socquet et al., 2006).

One of the main structures that connect the subduction zone in northern Sulawesi with deformation zone of the Banda Sea is Central Sulawesi Fault System (CSFS). As part of an active structure in Sulawesi Island, the seismic activity on the CSFS recorded both from the global and local seismic network is predominantly located in the shallow crustal zone (Bellier et al., 1998; Beaudouin et al., 2003). According to geodetic studies, paleomagnetic and other approaches, this active deformation is inferred to experience a high slip rate of about 30 to 50 mm/year (Bellier et al., 1998; Silver et al., 1983; Walpersdorf et al., 1998; Surmont et al., 1994) which has led to at least two major earthquakes (Mw > 6.5) (see Fig. 1) in the early twenty-first century namely the 2017 Mw 6.6 Poso (e.g., Sianipar et al., 2021; Wang et al., 2019; Daniarsyad et al., 2021) and the 2018 Mw 7.5 Palu-Donggala earthquakes (e.g., Socquet et al., 2019; Song et al., 2019; Zhang et al., 2019).

The 2017 Mw 6.6 Poso earthquake, struck on May 29, characterized by normal faulting. It ruptured along the Tokorondo Fault in the eastern region of Central Sulawesi. This event stands as the most significant recorded instance of a normal-faulting earthquake in Central Sulawesi, suggesting prolonged strain accumulation along this fault (Daniarsyad et al., 2021). The occurrence of such normal-faulting mechanisms can be attributed to ongoing mass extrusion processes in the eastern part of Sulawesi since the Quaternary to the present day. This extended extrusion is thought to play a crucial role in generating substantial internal deformation within the Tokorondo Mountains near the Poso fault, gradually building up strain energy that is eventually released during normal-faulting earthquakes (Wang et al., 2019; Daniarsyad et al., 2021).

Within approximately a year following the Poso earthquake, the 2018 Mw 7.5 Palu-Donggala earthquake ruptured on the Palu-Koro fault, exhibiting a strike-slip mechanism. This earthquake was classified as a supershear earthquake, characterized by an exceptionally high rupture velocity of ~4.1 km/s (Socquet et al., 2019; Natawidjaja et al., 2021). Notably, this particular earthquake induced submarine landslides, leading to the formation of a local tsunami. The shape of Palu Bay and the shallowness of the coastline likely contributed to the amplification of the tsunami's height. Despite this, analyses using planar fault model to assess the static stress transfer resulting from the 2017 Mw 6.6 Poso earthquake (Wang et al., 2019; Daniarsyad et al., 2021; Sianipar et al., 2021; Liu and Shi, 2021) suggest that the Poso earthquake had minimal influence on triggering the 2018 Mw 7.5 Palu-Donggala earthquake.

The Poso fault zone is one of distinct deformation domains that spans the central Sulawesi active deformation. An analysis of fault kinematics within the Poso domain reveals stress variations encompassing both oblique reverse-slip faulting and oblique-to pure normal-slip faulting (Bellier et al., 2006). It is evidenced by occurrence of normal-faulting earthquakes (Mw > 5.5) in the eastern part of Central Sulawesi prior to the 2017 Mw 6.6 Poso earthquake (Wang et al., 2019; Daniarsyad et al., 2021). Historical seismicity in the Poso fault indicates an absent of large earthquakes (Mw > 6) since instrumental records became available.

To evaluate the impact of the Poso and Palu-Donggala earthquakes on the Poso fault, we analyse their Coulomb stress transfer. The Coulomb stress transfer imposed by these two major earthquakes can change the stress field as they can promote or inhibit the seismic activity in the surrounding area (Freed, 2005). Earthquake Coulomb stress transfer studies on San Andreas Fault (King et al., 1994; Harris, 1998; Stein et al., 1994), Anatolian Fault (Stein et al., 1997; Hubert-Ferrari et al., 2000; Nalbant et al., 1998, 2002) and Sumatran Fault (Rafie et al., 2023; McCloskey et al., 2005; Qiu and Chan, 2019) has successfully identified the potential damaging earthquakes. Therefore, it becomes interesting to investigate how the 2017 Poso and the 2018 Palu-Donggala earthquakes influence the stress accumulation on the Poso fault, since, based on the historical accounts and instrumental record, the Poso fault has never been experiencing large earthquake and remain inactive (see Fig. 1) as well as the earthquake interactions in central part of Sulawesi have not been thoroughly understood (Wang et al., 2019).

Numerous studies have calculated the Coulomb stress changes resulting from these two large earthquakes and imparted the distributed stress onto planar receiver fault (Daniarsyad et al., 2021; Gunawan et al., 2020; Sianipar et al., 2021; Wang et al., 2019). However, the fault maps of Sulawesi Island show non-planar surface fault traces (see PUSGEN, 2017; Hall and Wilson, 2000; Socquet et al., 2006; Bellier et al., 2006), rendering the use of planar models for receiver faults inaccurate representations of fault geometry at depth. Prior studies have attempted to

address variable fault geometry, including the application of triangular dislocation elements (Parsons et al., 1999; Meade, 2007; Bie and Ryder, 2014; Rafie et al., 2022). In this study, we integrate variable receiver fault geometry into the Coulomb stress calculation triggered by the 2017 Mw 6.6 Poso and the 2018 Mw 7.5 Palu-Donggala earthquakes, aiming to conduct a detailed coseismic stress analysis on the Poso fault. Additionally, we consider the tectonic stress rate resulting from triple-junction convergence plate motion on Sulawesi Island. By combining stress changes model from large earthquakes and tectonic stress rates, we estimate stress accumulation on the Poso fault to enhance understanding of its potential for reactivation.

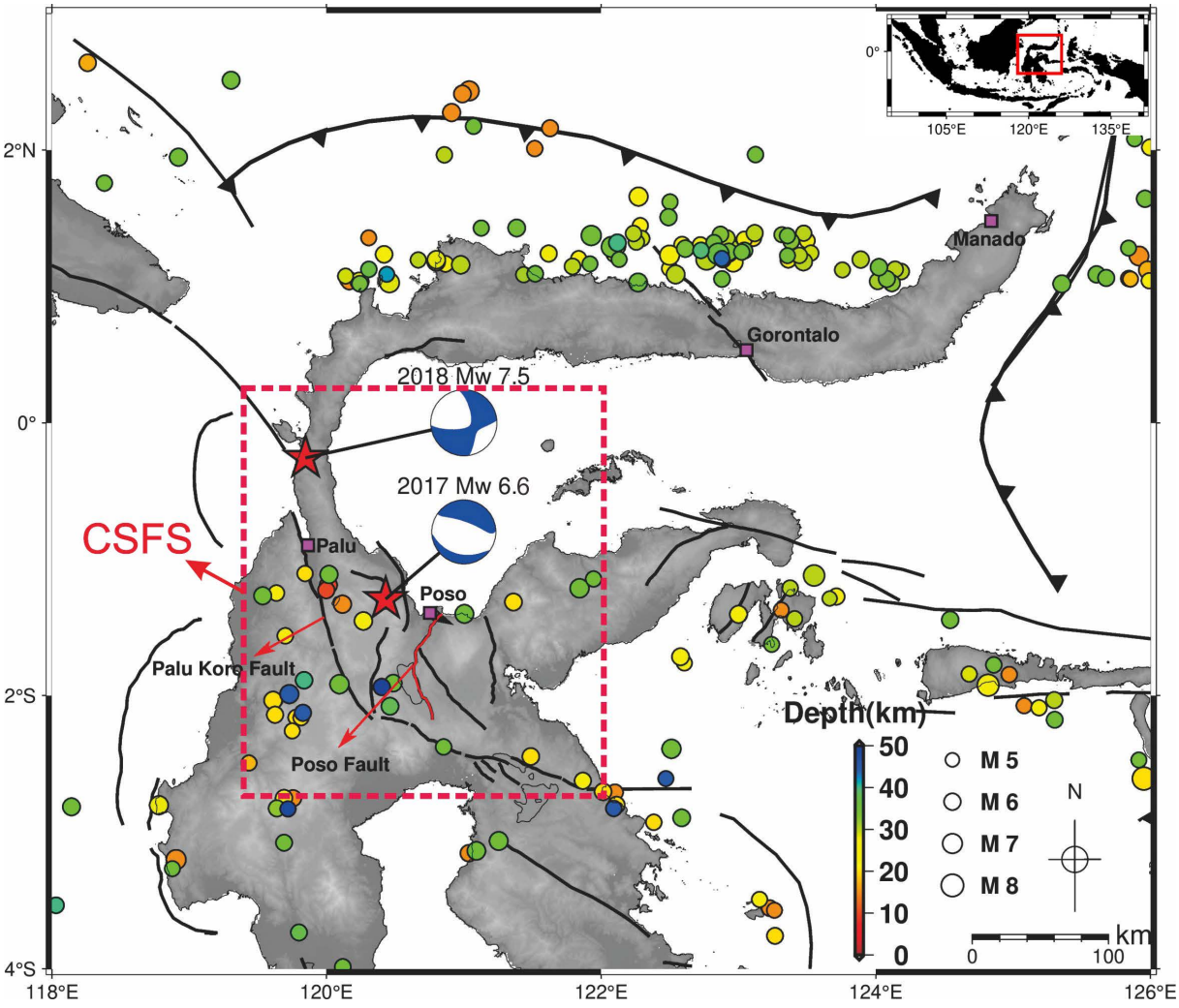

Figure 1. Seismicity of Sulawesi Island along with the focal mechanisms of the 2017 Mw 6.6 Poso and 2018 Mw 7.5 Palu–Donggala earthquakes. The red stars indicate the hypocenter locations of the Poso and Palu earthquakes. The coloured bar scale represents the hypocenter depth. The dashed box highlights the Central Sulawesi Fault System (CSFS), stretching south-eastward and covering the Palu-Koro and Matano faults. The Focal mechanisms of these two earthquakes were obtained from Global Centroid Moment Tensor (Dziewonski et al., 1981; Ekström et al., 2012). The seismicity data was obtained from the ISC-GEM catalogue (Di Giacomo et al., 2018; Storchak et al., 2015). The inset box shows the Island of Sulawesi, with the focus study area indicated by red box.

2. Finite fault models and multi-strike geometry of receiver fault

To analyse the interaction of the effects of large earthquakes on inland faults, we estimate the changes in stress on the Poso fault that includes coseismic stress transfer caused by the 2017 Poso and the 2018 Palu-Donggala earthquakes, plus interseismic stress loading from plate convergence coupling. In modelling the stress changes

caused by large inland earthquakes, we implement the finite fault slip models from previous studies. The 2017 Mw 6.6 Poso earthquake was taken from Wang et al. (2019) which was constructed based on coseismic displacement from InSAR data and the 2018 Mw 7.5 Palu-Donggala earthquake was taken from USGS (2018) which implemented the finite fault inverse algorithm for 40 teleseismic broadband waveforms data (Ji et al., 2002).

The Coulomb stress changes may be calculated either by imparting onto receiver fault with multi-variable geometry (e.g., Toda et al., 2011; Toda and Stein, 2020; Mildon et al., 2019) or onto optimally orientated planes (e.g., King et al., 1994). In this study, we consider the first approach since the Poso fault known to be a bending fault. The use of variable fault geometry parameters (strike, dip, and slip direction) has not been routinely included within Coulomb modelling. Therefore, to assess the Coulomb stress calculation, we segmented the Poso fault into 20 segments based on multi-strike parameters. According to PUSGEN (2017), the Poso fault is considered as a pure thrust fault, thus we assumed the dip and rake to be 45° and 90°, respectively. Aside from the choice of a dip value of 45°, we also consider the dip value of 25° as this value was found on a thrust fault in Indonesia (see Fernandez-Blanco et al., 2016) and compare the results. The fault geometry for each segment on the Poso fault is summarized in Table 1 and shown on Fig. 2. The choice of model faults with variable geometry can greatly improve the Coulomb stress estimation as it demonstrated by Mildon et al. (2019), where they investigated the Coulomb

No	Name	Strike (°)	Length (km)
1	Segment 1	246	2.5
2	Segment 2	218	6.4
3	Segment 3	211	2.4
4	Segment 4	230	2.4
5	Segment 5	190	6.4
6	Segment 6	218	9.6
7	Segment 7	226	4.7
8	Segment 8	205	4.8
9	Segment 9	174	7.3
10	Segment 10	207	4.7
11	Segment 11	175	3.5
12	Segment 12	186	2.2
13	Segment 13	152	2.4
14	Segment 14	163	11.5
15	Segment 15	149	3.0
16	Segment 16	163	3.3
17	Segment 17	114	3.0
18	Segment 18	149	4.9
19	Segment 19	162	8.5
20	Segment 20	176	4.7

Table 1. Fault geometry on each segment of the Poso fault based on multi-strike parameter.

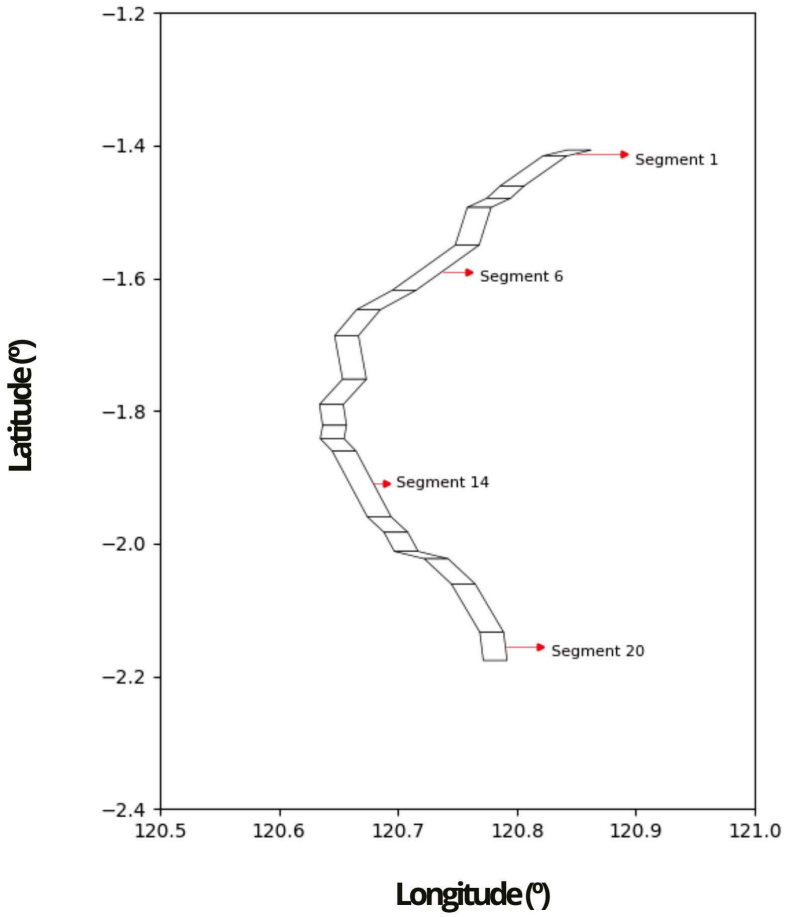

Figure 2. The segmentation of the Poso fault based on multi-strike parameter.

stress model on bending faults. They summarized that a long-strike fault bends on receiver faults would amplify or diminish the Coulomb stress when compared to adjacent regions of the fault. If the fault bends are not assessed, then the Coulomb stress model may not resolve critical areas with increased or decreased stress at bends that may associate with subsequent future earthquakes. In other words, the modelling of fault bends is one of the vital factors for earthquake triggering and hazard.

3. Methods

3.1 Change in Coulomb failure stress due to the 2017 Poso and the 2018 Palu-Donggala earthquakes

The principle of Coulomb failure criteria is frequently used to characterize the failure of a pre-existing fault, linking the shear stress acting on the fault to the normal stress (King et al., 1994). The changes in the static Coulomb Failure Stress (ΔCFS) have been applied to interpret the spatial arrangement of aftershock sequences or earthquakes induced by a major event (e.g., King et al., 1994; Stein, 1999). ΔCFS is characterized as:

$$\Delta CFS = \Delta\tau + \mu(\Delta\sigma + \Delta P) \quad (1)$$

Where $\Delta\tau$ is the shear stress change on a fault (positive in the slip direction), μ is the friction coefficient, $\Delta\sigma$ is the change in normal stress (positive in extension) and ΔP is the pore pressure change. In order to approximate the effects of pore pressure changes in ΔCFS, the medium is assumed to be homogeneous and isotropic (Harris, 1998).

Then, following Rice and Cleary (1976) and Roeloffs (1988), for the undrained situation of poroelastic medium, the pore pressure change is related to the mean stress change ΔP by:

$$\Delta P = -\beta' \Delta\sigma_{kk}/3 \tag{2}$$

Where β' for rock resembles to the Skemptons's (1954) coefficient β that was determined for soils. It depends upon the bulk modulii of the material and the proportion of volume occupied by the fluid (Rice and Cleary, 1976; Harris, 1998). σ_{kk} is the sum of the diagonal elements of the stress tensor. By assuming the change in the mean stress is proportional to the normal stress change (see Cocco and Rice, 2002; Cattin et al., 2009):

$$\beta' \Delta\sigma_{kk}/3 = \beta' \Delta\sigma \tag{3}$$

Eq. (1) is generally redefined as:

$$\Delta CFS = \Delta\tau + \mu' \Delta\sigma \tag{4}$$

Where $\mu' = \mu(1 - \beta')$ is the effective friction coefficient. By using Coulomb failure, the increased static stress will bring the fault closer to failure than it was prior to the large earthquake, while decreased static stress will delay the time it takes for the long-term tectonic loading to recover the static stress change (Harris, 1998). We used the COULOMB 3.4 code (Lin and Stein, 2004; Toda et al., 2005) to calculate ΔCFS of the 2017 Poso and the 2018 Palu-Donggala earthquakes using the elastic dislocation approach (Okada, 1985, 1992) and imparted the Coulomb stress for the specific orientation of each of the 20 segments on the Poso fault considered here.

The effective friction coefficient (μ') employed in the ΔCFS calculation was set at 0.1 and 0.4. A μ' value of 0.1 was chosen to align with studies of major pre-existing crustal fault system (see Hori and Oike, 1999; Shikakura et al., 2014), whereas a μ' of 0.4 is a commonly used value in computing ΔCFS (King et al., 1994; Pollitz et al., 2006; Nalbant et al., 2005; Qiu and Chan, 2019). We then calculate ΔCFS starting at 5 km depth up to 25 km depth with spacing of 5 km depth due to the shallow crustal earthquake hypocenter on Sulawesi Island is generally located in that particular area or known as seismogenic zone (PUSGEN, 2017).

The role of fault geometry is important to consider in evaluating the Coulomb stress, as has been illustrated by previous studies (e.g., Mildon et al., 2016, 2019; Sgambato et al., 2020; Rafie et al., 2023). Their studies explain that Coulomb stress calculation is most sensitive to the change in strike parameter rather than dip and rake parameters. Therefore, for bending fault like the Poso fault, we perform sensitivity tests for three different geometry models: planar, two-segmentation, and multi-strike variable geometries. These fault geometries demonstrate the sensitivity of the varying strike of receiver faults as it is expected to alter the stress distribution along-strike fault bends. The 2017 Mw 6.6 Poso earthquake is used as an example to calculate the static ΔCFS onto the Poso fault and to compare the planar and two types of variable fault geometry approach. We set the effective friction coefficient μ' to be 0.4 and start the depth from 5 km to 25 km. For the receiver faults (except the planar one), the strike parameter is varied individually, while the other two parameters are kept constant. The ΔCFS will be calculated using the assumption of pure thrust fault (dip of 45° and rake of 90°). The sensitivity test of ΔCFS on the Poso fault is portrayed in Fig. 3.

For the planar geometry (Fig. 3a), positive ΔCFS was primarily concentrated in the upper center of the fault, ranging from 5 km to 10 km depth, while negative ΔCFS was predominantly concentrated on the northern part of the fault across intermediate to deeper depths. In case of two-segmentation (Fig. 3b), where the bending point is located near the central part of the fault, high positive ΔCFS was observed exclusively on the northern side of the bending point at shallower depths (5 km to 10 km). Conversely, negative ΔCFS was concentrated at the edge of the northern side of the fault, expanding as it deepened on the northern side of the bending point. With the application of a multi-strike fault geometry (Fig. 3c), the distribution of ΔCFS became more varied. Positive ΔCFS was observed in the central-to-northern part of the fault, extending to deeper sections, while negative ΔCFS was concentrated at the tip of the northern part of the fault. Additionally, some negative ΔCFS was found at shallower depths in the

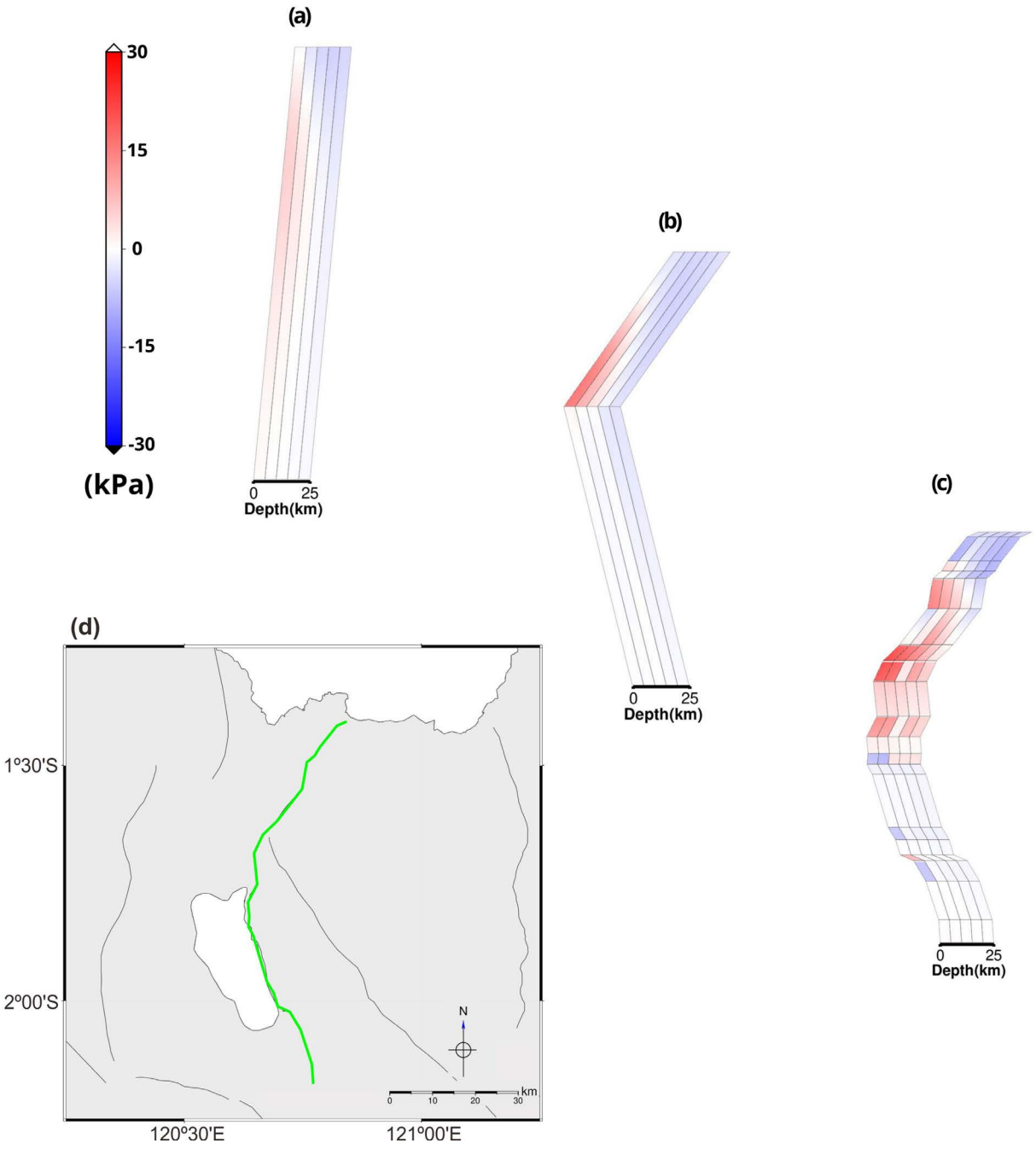

Figure 3. The static ΔCFS models on the Poso fault caused by the 2017 Poso earthquake with three different geometry models: (a) Planar geometry, (b) two-segmentation geometry, (c) a multi-strike geometry following (d) the real condition of the Poso fault geometry. The green bending line represents the surface trace of the Poso fault.

southern part of the fault. This test reveals that the role of fault geometry significantly influences the calculation of ΔCFS. If the standard planar fault approach is used, the positive ΔCFS at greater depths would be diminished, as also evidenced when employing the two-segmentation fault geometry approach. This suggests that the stress distribution on these fault sections would be incorrectly resolved, leading to a misinterpretation of the resulting models.

3.2 Tectonic stress rate estimation

The rate of tectonic stress is a significant factor influencing stress changes leading to earthquake occurrences on a fault. A higher tectonic stress rate can accelerate the recovery of stress accumulation on the fault to its critical

condition following an earthquake, while a lower rate can slow down this process (Hori and Oike, 1999). We assumed the tectonic stress rate comes from the coupling of the triple-junction convergence rate of Indo-Australia, Philippine Sea, and Sunda plates where the relative motion in the central part of Sulawesi is accommodated by left-lateral strike-slip motion along the Matano fault and continues to the Palu Koro fault in the north (Socquet et al., 2006). Based on the generalized Hooke's law, the relationship between the stress rate (σ') and strain (ε') rate tensor components in 2D plane can be defined in matrix form as follow:

$$\begin{bmatrix} \boldsymbol{\sigma'_{xx}} \\ \boldsymbol{\sigma'_{yy}} \\ \boldsymbol{\sigma'_{xy}} \end{bmatrix} = \frac{\boldsymbol{E}}{(\mathbf{1}+\boldsymbol{v})(\mathbf{1}-\mathbf{2}\boldsymbol{v})} \begin{bmatrix} (\mathbf{1}-\boldsymbol{v}) & \boldsymbol{v} & \mathbf{0} \\ \boldsymbol{v} & (\mathbf{1}-\boldsymbol{v}) & \mathbf{0} \\ \mathbf{0} & \mathbf{0} & (\mathbf{1}-\mathbf{2}\boldsymbol{v}) \end{bmatrix} \begin{bmatrix} \boldsymbol{\varepsilon'_{xx}} \\ \boldsymbol{\varepsilon'_{yy}} \\ \boldsymbol{\varepsilon'_{xy}} \end{bmatrix} \tag{5}$$

Where $\boldsymbol{E}$ and $\boldsymbol{v}$ are the Young's modulus and Poisson's ratio, respectively.

We used geodetic plate motion from Kreemer et al. (2014) through the GSRMv2.1 to obtain the strain rate at the coordinate 1.75°S and 120.90°E (see Fig. S1). By assuming $\boldsymbol{E}$ is 80 GPa and $\boldsymbol{v}$ is 0.25 (Lin and Stein, 2004; Toda et al., 2005), we get the stress rate tensor components to be:

$$\begin{bmatrix} -3.69\ kPa/yr \\ 6.31\ kPa/yr \\ -0.97\ kPa/yr \end{bmatrix} = \frac{\mathbf{80\ GPa}}{(\mathbf{1}+\mathbf{0.25})(\mathbf{1}-\mathbf{2}*\mathbf{0.25})} \begin{bmatrix} (\mathbf{1}-\mathbf{0.25}) & \mathbf{0.25} & \mathbf{0} \\ \mathbf{0.25} & (\mathbf{1}-\mathbf{0.25}) & \mathbf{0} \\ \mathbf{0} & \mathbf{0} & (\mathbf{1}-\mathbf{2}*\mathbf{0.25}) \end{bmatrix} \begin{bmatrix} -67.9\ nanostrain/yr \\ 88.4\ nanostrain/yr \\ -15.1\ nanostrain/yr \end{bmatrix} \tag{6}$$

The stress rate tensor components are then evaluated to extrapolate the corresponding principal stress rates (σ'_1, σ'_2) by determining its eigenvalues. We then compute the normal and shear stress rate changes using Coulomb-failure criterion using the equation as follow:

$$\sigma'_N = \frac{1}{2}(\sigma'_1 + \sigma'_2) - \frac{1}{2}(\sigma'_1 - \sigma'_2)\cos 2\theta \tag{7}$$

$$\sigma'_S = \frac{1}{2}(\sigma'_1 - \sigma'_2)\sin 2\theta \tag{8}$$

Where θ is the angle between the direction of the surface normal on a plane and the orientation of the maximum principal stress, and σ'_N and σ'_S are normal and shear stress rates, respectively. Solving these equations yields $\begin{bmatrix} \sigma'_N \\ \sigma'_S \end{bmatrix} = \begin{bmatrix} 6.13\ kPa/yr \\ -0.017\ kPa/yr \end{bmatrix}$. By employing Eq. (4) and assuming μ' is 0.4, the tectonic stress rate is ~2.4 kPa/yr.

4. Results and Discussion

4.1 The effect of ΔCFS imparted by the 2017 Poso and the 2018 Palu-Donggala earthquakes on the Poso fault

The results for ΔCFS of the 2017 Poso and the 2018 Palu-Donggala earthquake calculated on the Poso fault are shown in Figs. 4 and 5, respectively. The ΔCFS distribution on the Poso fault due to the 2017 Poso earthquake (Fig. 4) from two parameters μ' and dips generated relatively similar which positive ΔCFSs of 5 kPa to 27 kPa are concentrated around the center segments of the fault that are segment 5-11, while negative ΔCFSs of −8 kPa to −2 kPa are found on the northern part of the Poso fault (segment 1-5). The same results also occurred when modeling the stress transfer caused by the 2018 Palu-Donggala earthquake (Fig. 5) where all segments around the northern part of the Poso fault are predominantly experienced negative ΔCFS of > −16 kPa.

In explaining the influence of the 2017 Poso and the 2018 Palu-Donggala earthquakes into the Poso fault, we estimated the accumulation of ΔCFS imparted by those two events (Figs. 4 and 5). We displayed their cumulative values on multi-segments of the Poso fault in Fig. 6. The distribution of the cumulative ΔCFS along the Poso fault exhibits a high negative value in the north (segment 1 – segment 4) of up to −20 kPa and moderate negative value in

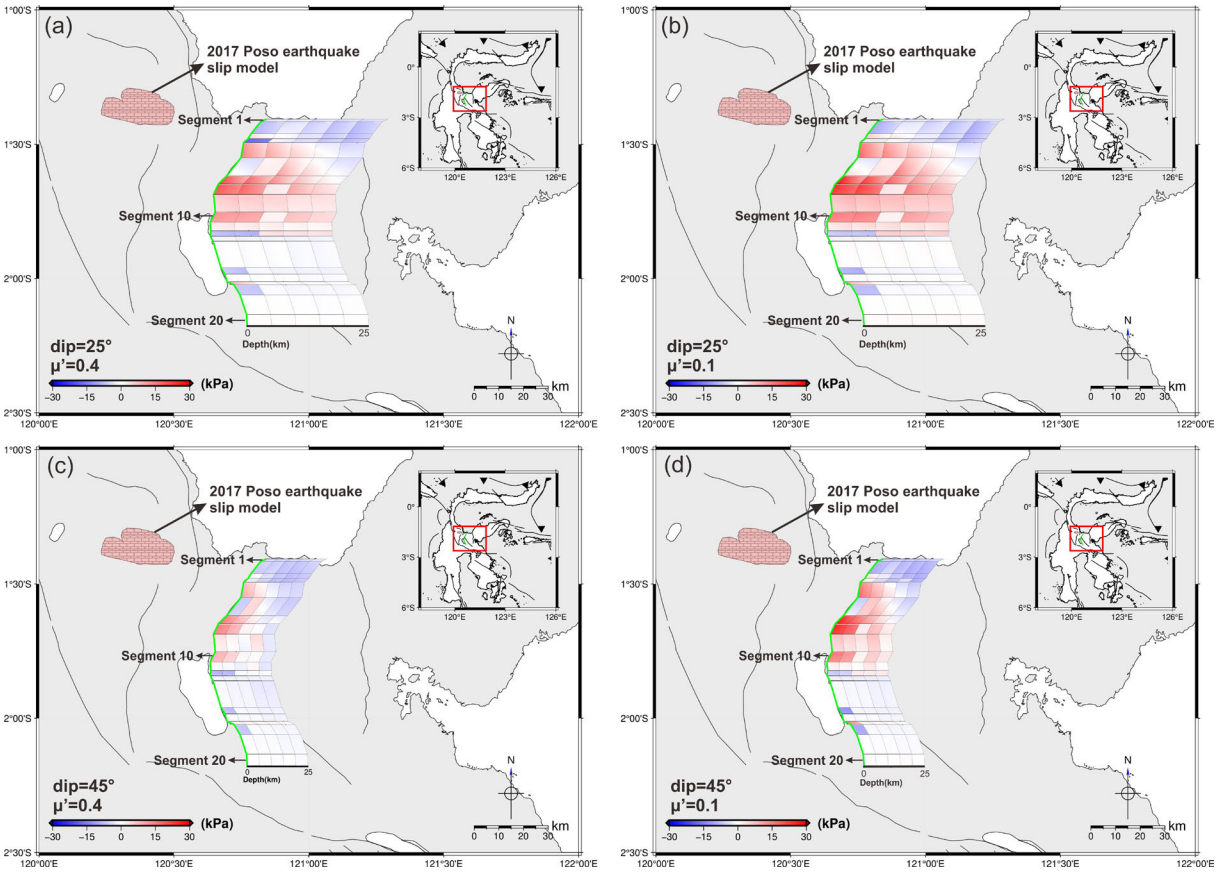

Figure 4. Static coseismic ΔCFS of the 2017 Poso earthquake. (a) ΔCFS with μ' of 0.4 and dip of 25°, (b) ΔCFS with μ' of 0.1 and dip of 25°, (c) ΔCFS with μ' of 0.4 and dip of 45°, and (d) ΔCFS with μ' of 0.1 and dip of 45°. The filled light pink polygon shows the slip area > ~2 m of the 2017 Poso earthquake. The green bending line represents the surface trace of the Poso fault. The inset box shows the Island of Sulawesi, with the focus study area indicated by red box.

the center (segment 5 – segment 11) of up to −5 kPa. To analyse more in detail the effect of large inland earthquakes on each segment of the Poso fault, we investigate their values on each parameter of μ' and dip. When we used $\mu' = 0.4$ and 0.1 with dip = 25° (Fig. 4a and 4b) for ΔCFS calculation of the 2017 Poso earthquake, at segment 10, it exhibits similar positive ΔCFS on each depth. However, dip = 45° produced negative ΔCFS > ~−2 kPa at 20 km-25 km depth (Fig. 4c and 4d). This pattern is also found on other segments, such as segments 8, 9, 11 and 12.

For the ΔCFS calculation of the 2018 Palu-Donggala earthquake using $\mu' = 0.4$ and 0.1 with dip = 25° (Fig. 5a and 5b), segments 1-12 exhibit high negative ΔCFS > −10 kPa, remarkably similar to the pattern following dip = 45° (Fig. 5c and 5d). Only Fig. 5c that exhibits smaller negative ΔCFS than any other combined parameters. However, despite the dominantly negative ΔCFS imparted by the 2018 Palu-Donggala earthquake, the positive ΔCFSs are identified when using $\mu' = 0.4$ and dip = 45° (Fig. 5c) at lower depth on the southern part of Poso fault (segment 13, 15, 16, 18, and 19) with ΔCFS > 0.1 kPa.

The cumulative ΔCFS displayed in Fig. 6 also yields almost similar pattern for different parameters of μ' and dip. The ΔCFS results in Fig. 6a and 6b exhibit similar pattern with high negative ΔCFS > ~−20 kPa on the north and low negative ΔCFS > ~−5 kPa. Only when using dip = 45° (Fig. 6c and 6d), some segments experience positive ΔCFS, for instance, for $\mu' = 0.1$ (Fig. 6d), the positive ΔCFS of ~5 kPa recorded on segment 17 at 5 km depth and for $\mu' = 0.4$ (Fig. 6c), the positive ΔCFSs are identified in segment 9 at 20 km depth and segment 10 at 5 km depth of around 1 kPa. Based on the cumulative results of those two large events, it can be seen that the influence of the 2018 Palu-Donggala earthquake is much stronger than the 2017 Poso earthquake. This is certainly caused by the difference in magnitude where the 2018 Palu-Donggala earthquake produced Mw 7.5, almost an approximate logarithmic divergence of one unit in contrast to the magnitude produced by the 2017 Poso earthquake. The cumulative ΔCFS results also transferred the negative ΔCFS in almost the entire segment of the Poso fault (from ~−5 kPa to ~−10 kPa) meaning that their effects have moved the Poso fault away from failure, or potentially delayed failure.

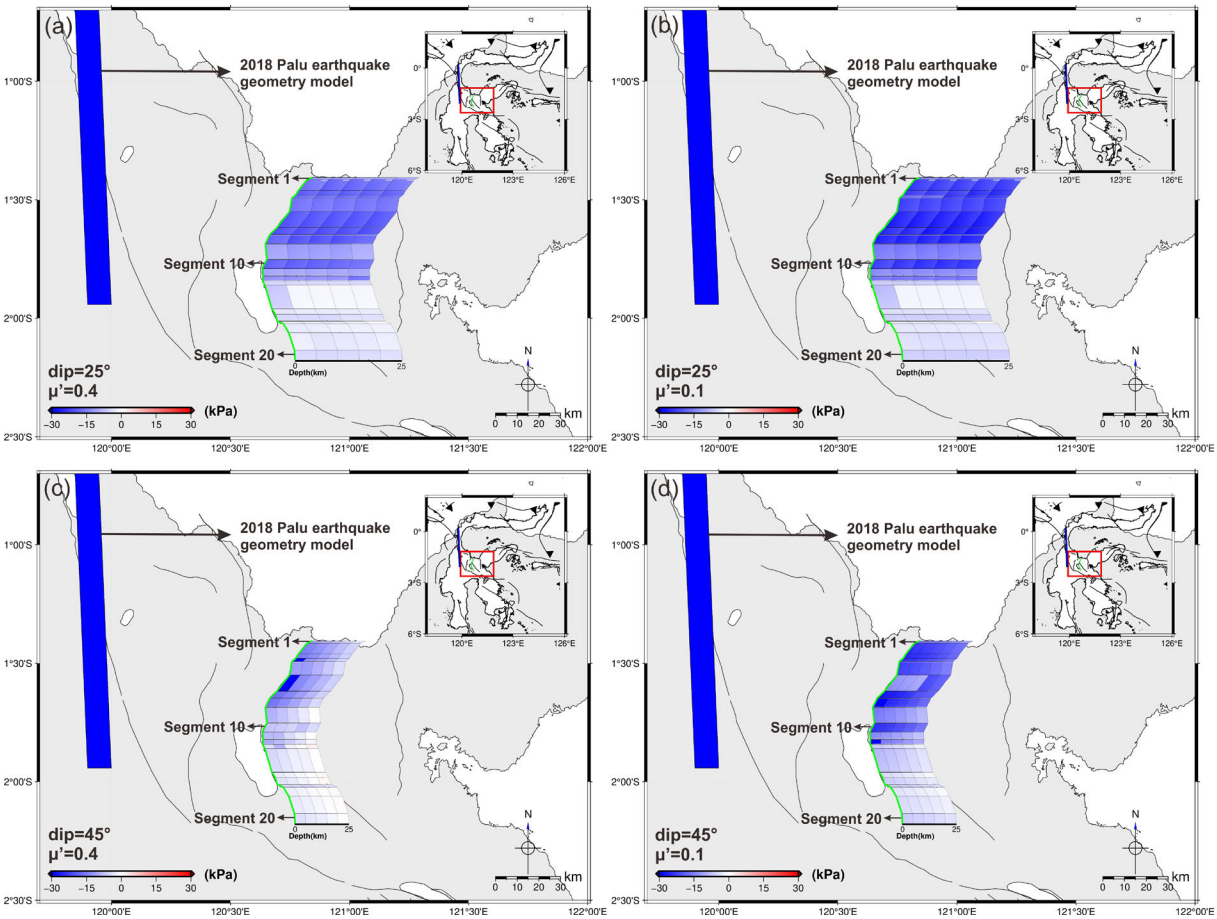

Figure 5. Static coseismic ΔCFS of the 2018 Palu-Donggala earthquake. (a) ΔCFS with μ' of 0.4 and dip of 25°, (b) ΔCFS with μ' of 0.1 and dip of 25°, (c) ΔCFS with μ' of 0.4 and dip of 45°, and (d) ΔCFS with μ' of 0.1 and dip of 45°. The green bending line represents the surface trace of the Poso fault. The inset box shows the Island of Sulawesi, with the focus study area indicated by red box. The filled blue long rectangle, pointed by the black arrow, portrays the geometry model of the 2018 Palu-Donggala earthquake.

4.2 ΔCFS time function on the Poso fault

In modeling the ΔCFS time function on the Poso fault, we combine the results of ΔCFS due to large inland earthquakes and the tectonic stress rate as this model has been presented in other stress evolution studies on Sumatran Fault (see Rafie et al., 2023), SW Japan (Hori and Oike, 1999; Shikakura et al., 2014; Mitogawa and Nishimura, 2020) and Palu Koro fault (Liu and Shi, 2021).

We model the ΔCFS time function in a range of 20 years, from 2010-2030 where the 2017 Poso and the 2018 Palu-Donggala occurred in that period of time. We used the ΔCFS model resulted from using $\mu' = 0.4$ and dip = 25° at 10 km depth. The ΔCFS time function model is shown in Fig. 7, other models that use different combinations of μ' and dip can be seen in Figs. S2, S3, and S4. The tectonic stress rate of 2.4 kPa on the Poso fault estimated in this study is roughly similar to the result obtained by Liu and Shi (2021), where their estimation the tectonic stress rate around Sulawesi Island to be 3.6 kPa. Also, this value is similar to that obtained in SW Japan's Nankai Trough forearc by Shikakura et al. (2020) and Mitogawa and Nishimura (2020) as well as in Sumatran Fault with the case of no sliver movement (see Rafie et al., 2023), which suggests a low rate of tectonic loading.

Based on Fig. 7, high negative ΔCFSs due to the 2018 Palu-Donggala earthquake are concentrated around the northern part of the Poso fault at segments 1-12 ranging from −20 kPa to −10 kPa and low negative stress in the south at segment 13-20 with ΔCFS > −3 kPa. The 2017 Poso earthquake transferred low negative stress as low as > ~−3 kPa in the north (segment 1-4) and south (segment 12-20) of the Poso fault, while high positive ΔCFSs of > ~10 kPa are found in the center of the fault (segment 5-11). Due to the high-stress release by the 2018

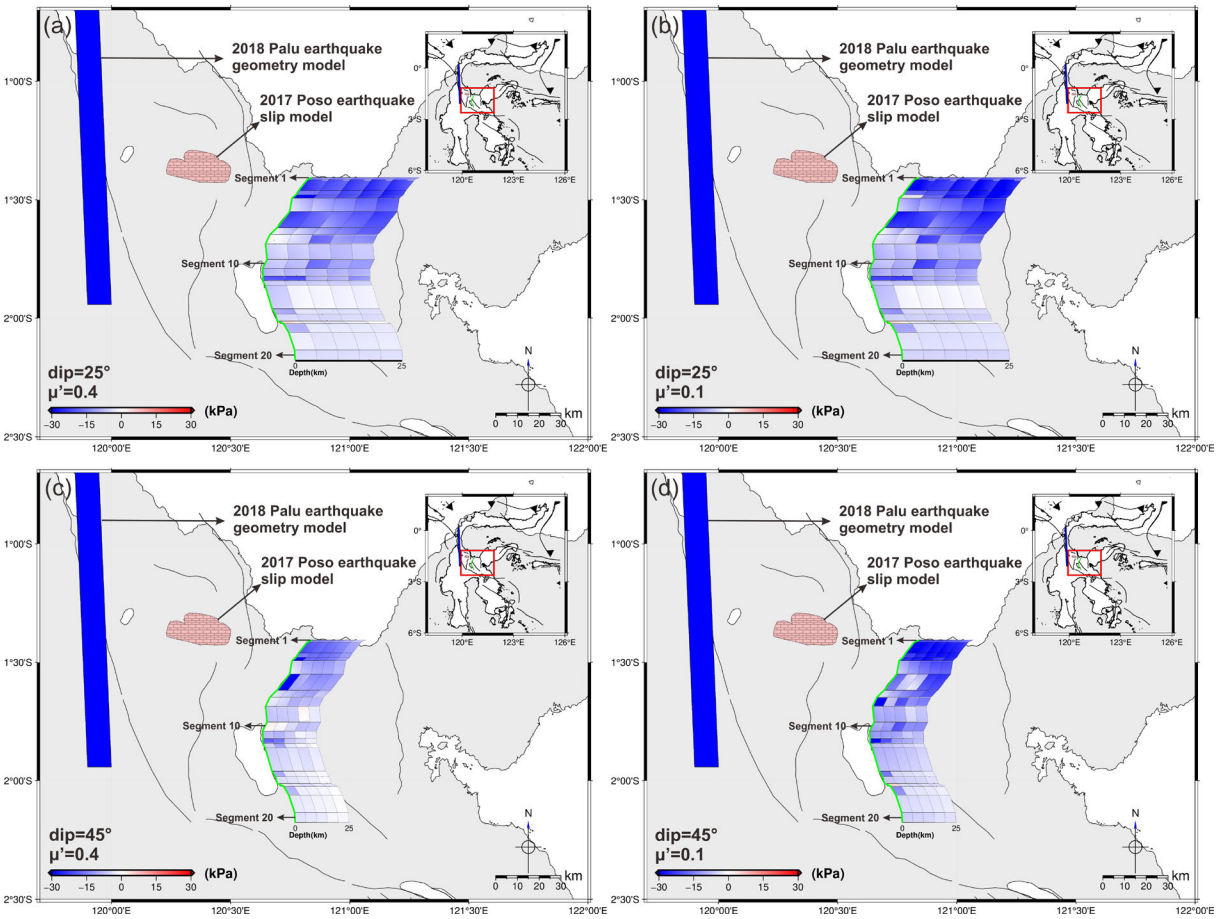

Figure 6. Cumulative static coseismic ΔCFS from the 2017 Poso and the 2018 Palu-Donggala earthquakes. (a) ΔCFS with μ' of 0.4 and dip of 25°, (b) ΔCFS with μ' of 0.1 and dip of 25°, (c) ΔCFS with μ' of 0.4 and dip of 45°, and (d) ΔCFS with μ' of 0.1 and dip of 45°. The filled light pink polygon shows the slip area > ~2 m of the 2017 Poso earthquake. The green bending line represents the surface trace of the Poso fault. The inset box shows the Island of Sulawesi, with the focus study area indicated by a red box. The filled blue long rectangle, pointed by the black arrow, portrays the geometry model of the 2018 Palu-Donggala earthquake.

Palu-Donggala earthquake in comparison with the 2017 Poso earthquake, its coseismic stress change drops the stress accumulation on segments 1-4, 6, and 11-12, so that it inhibits these segments to bring forward to their critical condition. For segments 5 and 7-10, positive ΔCFS resulting from the 2017 Poso earthquake and negative ΔCFS arising from the 2018 Palu-Donggala earthquake exhibit nearly equivalent magnitudes, so that their effects cancel each other out. Other segments in the south (segments 13-20) experience the lowest coseismic ΔCFSs by these two large earthquakes.

From these analyses, we infer that the effect of large earthquakes sufficiently controls the stress accumulation within the northern to central segments of the Poso fault. In contrast, because there is no historical record of significant earthquake on the southern part of Sulawesi earthquake, the southern portion of the Poso fault might be more distinctly governed by the tectonic stress rates (see Fig. 8). For overall ΔCFS time function models along the Poso fault displayed in Fig. 7, it is evident that the southernmost segment of the Poso fault exhibits the highest stress accumulation, suggesting a potential advancement toward critical conditions. However, determining the specific segments on the Poso fault that may have advanced to critical thresholds remains difficult to constrain due to the paucity of historical large earthquakes and the limited understanding of fault strength characteristics along the Poso fault. Furthermore, the absence of large earthquakes on this fault suggests the potential presence of creeping, akin to those observed along the Aceh fault. Despite its high-stress accumulation, the fault experiences creep and has yet to produce an earthquake with M > 7.0 (Rafie et al., 2023; Ito et al., 2012; Tong et al., 2018). Nonetheless, further investigations are requisite to substantiate this assertion, particularly through geodetic and geological observations.

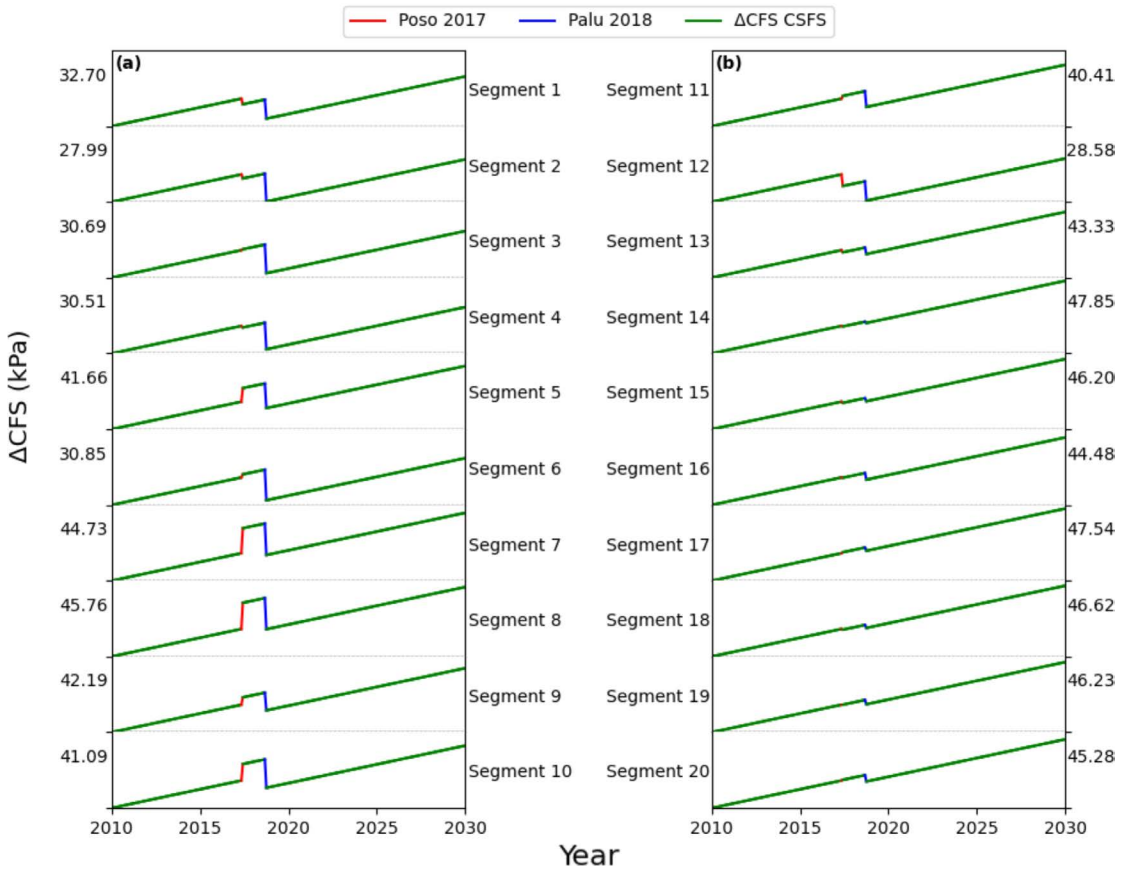

Figure 7. ΔCFS time function on each Poso fault segment, (a) for segment 1-10 and (b) for segment 11-20. Coseismic changes in CFS due to the occurrence of the 2017 Poso and the 2018 Palu-Donggala earthquakes (blue and red lines, respectively) as well as the tectonic stress rate (green) around Central Sulawesi Fault System (CSFS) are indicated. The absolute value of the range of change in CFS (kPa) from these sources, accumulated over 20 years for each segment is indicated on the left of (a) and the right of (b).

5. Conclusion

We have assessed the impact of the 2017 Poso and the 2018 Palu-Donggala earthquakes on the multi-strike segments of the Poso fault, including an estimation of the tectonic stress rate due to triple-junction plate convergence beneath Sulawesi Island.

The effect of coseismic ΔCFS on the Poso fault suggests that the northern segments undergo a considerably high amount of negative stress changes, which potentially extends these segments toward critical conditions, while the southern portion experiences a comparatively lesser effect. The cumulative ΔCFS of both large earthquakes implies a prevailing influence of the 2018 Palu-Donggala earthquake in comparison to the 2017 Poso earthquake.

Derived from the ΔCFS time function models, it becomes apparent that the ΔCFS resulting from large earthquakes within the northern to central segments of the Poso fault modulates the stress accumulation within that region. Conversely, the southern segments of the Poso fault exhibit a stress distribution that lack significant impact, thus highlighting the dominant role of tectonic stress rates in amplifying stress accumulation in this area. The notable stress buildup in the Poso fault potentially signifies an advancement towards critical conditions, thereby enhancing seismic hazards within this location.

This study also demonstrates that the stress accumulation model of the Poso fault overlooks the intricate geometry of its individual segments, which may exhibit varying dip, rake values, and possibly oblique motion. Our approach to estimating tectonic stress rate is simplified by employing the nearest strain rate model to the Poso fault rather than addressing each segment separately. To generate a more accurate ΔCFS time function model, the calculation should incorporate postseismic motion or viscoelastic function, a factor which has not been addressed in this study. Although these effects are notably significant in the aftermath of major earthquake, our study focuses

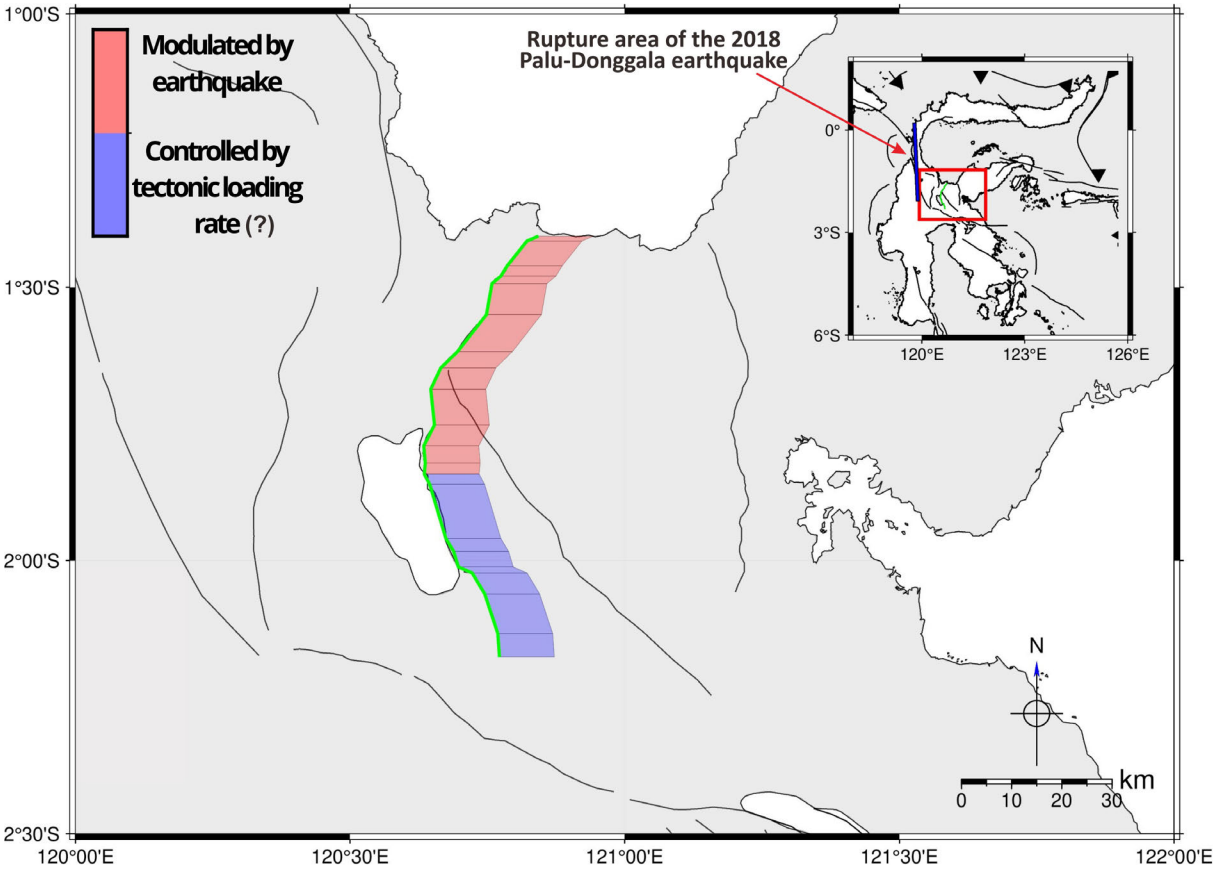

Figure 8. Illustration of large earthquake and tectonic stress rate influences on each segment of the Poso fault. The green bending line represents the surface trace of the Poso fault. The filled red segments indicate that coseismic ΔCFS sufficiently modulate the stress accumulation, while the filled blue segments show that the tectonic loading rate might dominantly control the stress accumulation. The inset box shows the Island of Sulawesi with the focus study area indicated by the red box. The filled blue long rectangle, pointed by the red arrow, portrays the rupture area of the 2018 Palu-Donggala earthquake.

on events with $M < 7.6$, making postseismic effects less impactful and does not affect our findings. Nonetheless, we posit that the stress accumulation model developed herein can serve as an initial reference for modeling stress distribution on Sulawesi Island. Furthermore, it can be applied in future seismic hazard assessments and research, including its application in evaluating earthquake risk mitigation strategies in the surrounding region.

Data availability statement. The original contributions presented in the study are included in the article/supplementary material, and further inquiries can be directed to the corresponding author/s. The authors declare that the research was conducted in the absence of any commercial and financial relationships that could be construed as a potential conflict of interest. The authors have no relevant financial or non-financial interests to disclose. All authors contributed to the study conception and design. M.A.M contributed to conceptualize the study, preliminary design the study and supervise the final manuscript. M.T.R. contributed to conceive the study, draft the final manuscript, estimate the tectonic stress rate and evaluate all the results. T.R. contributed to the earthquake Coulomb stress estimation and draft the first manuscript. M.A.H.A, E.S., and M.M. contributed to supervise and validate the results. All authors contributed to the preparation of the manuscript. All authors read and approved the final manuscript.

Acknowledgments. This research was supported by the Hibah Penelitian Internal Fakultas MIPA of Hasanuddin University No. 994/UN4.11/PT.01.02/2023. The authors also thank anonymous reviewer(s) and Editor in Chief, and Enrico Serpelloni as Sector Editor, for their comments which help improved the quality of this manuscript. Figures were generated using Python and the Generic Mapping Tools (GMT) (Wessel et al., 2019).

References

Beaudouin, T., O. Bellier and M. Sebrier (2003). Present-day stress and deformation field within the Sulawesi Island area (Indonesia): geodynamic implications, Bull. Soc. Geol. Fr., 174, 3, 305-317, doi:10.2113/174.3.305.

Bellier, O., T. Beaudouin, M. Sébrier, I. Villeneuve et al. (1998). Active faulting in central Sulawesi (eastern Indonesia), GEODYSSEA project final report, 98-14.

Bellier, O., M. Sébrier, D. Seward, T. Beaudouin et al. (2006). Fission track and fault kinematics analyses for new insight into the Late Cenozoic tectonic regime changes in West-Central Sulawesi (Indonesia), Tectonophysics, 413, 3-4, 201-220, doi:10.1016/j.tecto.2005.10.036.

Bie, L. and I. Ryder (2014). Recent seismic and aseismic activity in the Ashikule stepover zone, NW Tibet, Geophys. J. Int., 198, 3, 1632-1643, doi:10.1093/gji/ggu230.

Cattin, R., N. Chamot-Rooke, M. Pubellier, A. Rabaute et al. (2009). Stress changes and effective friction coefficient along the Sumatra-Andaman-Sagaing fault system after the 26 December 2004 (Mw = 9.2) and the 28 March 2005 (Mw = 8.7) earthquakes, Geochem. Geophys. Geosyst., 10, 3, doi:10.1029/2008GC002167.

Cocco, M. and J. R. Rice (2022). Pore pressure and poroelasticity effects in Coulomb stress analysis of earthquake interactions, J. Geophys. Res. Solid Earth, 107, B2, ESE2-1 – ESE2-17, doi:10.1029/2000JB000138.

Daniarsyad, G., D. Sianipar, N. Heryandoko and P. Priyobudi (2021). Source mechanism of the 29 May 2017 Mw 6.6 Poso (Sulawesi, Indonesia) earthquake and its seismotectonic implication, Pure Appl. Geophys., 178, 8, 2807-2819, doi:10.1007/s00024-021-02779-y.

Di Giacomo, D., E. R. Engdahl and D. A. Storchak (2018). The ISC-GEM earthquake catalogue (1904-2014): status after the extension project, Earth Syst. Sci. Data, 10, 4, 1877-1899, doi:10.5194/essd-10-1877-2018.

Dziewonski, A. M., T. A. Chou and J. H. Woodhouse (1981). Determination of earthquake source parameters from waveform data for studies of global and regional seismicity, J. Geophys. Res. Solid Earth, 86, B4, 2825-2852, doi:10.1029/JB086iB04p02825.

Ekström, G., M. Nettles and A. M. Dziewonski (2012). The global CMT project 2004-2010: Centroid-moment tensors for 13,017 earthquakes, Phys. Earth Planet. Inter., 200, 1-9, doi:10.1016/j.pepi.2012.04.002.

Fernandez-Blanco, D., M. Philippon and C. von Hagne (2016). Structure and kinematics of the Sumatran fault system in North Sumatra (Indonesia), Tectonophysics, 693, 453-464, doi:10.1016/j.tecto.2016.04.050.

Freed, A. M. (2005). Earthquake triggering by static, dynamic, and postseismic stress transfer, Annu. Rev. Earth Planet. Sci., 33, 335-367, doi:10.1146/annurev.earth.33.092203.122505.

Gunawan, E., S. Widiyantoro, P. Supendi and T. Nishimura (2020). Identifying the most explainable fault ruptured of the 2018 Palu-Donggala earthquake in Indonesia using Coulomb failure stress and geological field report, Geod. Geodyn., 11, 4, 252-257, doi:10.1016/j.geog.2020.04.004.

Hall, R. and M. E. J. Wilson (2000). Neogene sutures in eastern Indonesia, J. Asian Earth Sci., 18, 781-808, doi:10.1016/S1367-9120(00)00040-7.

Harris, R. A. (1998). Introduction to special section: Stress triggers, stress shadows, and implications for seismic hazard. J. Geophys. Res., 103, 24347-24358, doi:10.1029/98JB01576.

Hori, T. and K. Oike (1999). A physical mechanism for temporal variation in seismicity in Southwest Japan related to the great interplate earthquakes along the Nankai trough, Tectonophysics, 308, 1-2, 83-98, doi:10.1016/S0040-1951(99)00079-7.

Hubert-Ferrari, A., A. Barka, E. Jacques, S. S. Nalbant et al. (2000). Seismic hazard in the Marmara Sea region following the 17 August 1999 Izmit earthquake, Nature, 404, 6775, 269-273, doi:10.1038/35005054.

Ito, T., E. Gunawan, F. Kimata, T. Tabei et al. (2012). Isolating along-strike variations in the depth extent of shallow creep and fault locking on the northern Great Sumatran Fault, J. Geophys. Res. Solid Earth, 117, B6, doi:10.1029/2011JB008940.

Ji, C., D. J. Wald and D. V. Helmberger (2002). Source description of the 1999 Hector Mine, California, earthquake, part I: Wavelet domain inversion theory and resolution analysis, Bull. Seismol. Soc. Am., 92, 4, 1192-1207, doi:10.1785/0120000916.

King, G. C. P., R. S. Stein and J. Lin (1994). Static stress changes and the triggering of earthquakes, Bull. Seismol. Soc. Am., 84, 935-953, doi:10.1785/BSSA0840030935.

Kreemer, C., G. Blewitt and E. C. Klein (2014). A geodetic plate motion and Global Strain Rate Model, Geochem. Geophys. Geosyst., 15, 10, 3849-3889, doi:10.1002/2014GC005407.

Lin, J. and R. S. Stein (2004). Stress triggering in thrust and subduction earthquakes and stress interaction between the southern San Andreas and nearby thrust and strike-slip faults, J. Geophys. Res. Solid Earth, 109, B2, doi:10.1029/2003JB002607.

Liu, C. and Y. Shi (2021). Space-time stress variations on the Palu-Koro fault impacting the 2018 Mw 7.5 Palu earthquake and its seismic hazards, Geochem. Geophys. Geosyst., 22, 5, e2020GC009552, doi:10.1029/2020GC009552.

McCloskey, J., S. Nalbant and S. Steacy (2005). Earthquake risk from co-seismic stress, Nature, 434, 291, doi:10.1038/434291a.

Meade, B. J. (2007). Algorithm for the calculation of exact displacements, strains, and stresses for triangular dislocation elements in a uniform elastic half space, Comput. Geosci., 33, 8, 1064-1075, doi:10.1016/j.cageo.2006.12.003.

Mildon, Z. K., S. Toda, J. P. Faure Walker and G. P. Robert (2016). Evaluating models of Coulomb stress transfer: is variable fault geometry important?, Geophys. Res. Lett., 43, 24, 12407-12414, doi:10.1002/2016GL071128.

Mildon, Z. K., G. P. Robert, J. F. Walker and S. Toda (2019). Coulomb pre-stress and fault bends are ignored yet vital factors for earthquake triggering and hazard, Nat. Commun., 10, 1, 2744, doi:10.1038/s41467-019-10520-6.

Mitogawa, T. and T. Nishimura (2020). Coulomb stress change on inland faults during megathrust earthquake cycle in southwest Japan, Earth Planets Space, 72, 1, 66, doi:10.1186/s40623-020-01174-6.

Nalbant, S. S., A. Hubert and G. C. P. King (1998). Stress coupling between earthquakes in northwest Turkey and the North Aegean Sea, J. Geophys. Res., 103, 24469-24486, doi:10.1029/98JB01491.

Nalbant, S. S., J. McCloskey, S. Steacy and A. A. Barka (2002). Stress accumulation and increased seismic risk in eastern Turkey, Earth Planet. Sci. Lett., 195, 291-298, doi:10.1016/S0012-821X(01)00592-1.

Nalbant, S. S., S. Steacy, K. Sieh, D. Natawidjaja et al. (2005). Earthquake risk on the Sunda trench, Nature, 435, 7043, 756-757, doi:10.1038/nature435756a.

Natawidjaja, D. H., M. R. Daryono, G. Prasetya, U. Udrekh et al. (2021). The 2018 Mw 7.5 Palu supershearh earthquake ruptures geological fault's multisegment separated by large bends: results from integrating field measurements, LiDAR, swath bathymetry and seismic-reflection data, Geophys. J. Int., 224, 2, 985-1002, doi:10.1093/gji/ggaa498.

Okada, Y. (1985). Surface deformation due to shear and tensile faults in a half-space, Bull. Seismol. Soc. Am., 75, 4, 1135-1154, doi:10.1785/BSSA0750041135.

Okada, Y. (1992). Internal deformation due to shear and tensile faults in a half-space, Bull. Seismol. Soc. Am., 82, 2, 1018-1040, doi:10.1785/BSSA0820021018.

Parsons, T., R. S. Stein, R. W. Simpson and P. A. Reasenberg (1999). Stress sensitivity of fault seismicity: A comparison between limited-offset oblique and major strike-slip faults, J. Geophys. Res. Solid Earth, 104, 20183-20202, doi:10.1029/1999JB900056.

Pollitz, F. F., P. Banerjee, R. Bürgmann, M. Hashimoto et al. (2006). Stress changes along the Sunda trench following the 26 December 2004 Sumatra-Andaman and 28 March 2005 Nias earthquakes, Geophys. Res. Lett., 33, 6, doi:10.1029/2005GL024558.

PUSGEN (2017). Indonesia's earthquake source and hazard map (in Bahasa Indonesia), Research and Development Agency of Ministry of Public Work and Housing, Indonesia, ISBN:978-602-5489-01-3.

Qiu, Q. and C. H. Chan (2019). Coulomb stress perturbation after great earthquakes in the Sumatran subduction zone: potential impacts in the surrounding region, J. Asian Earth Sci., 180, 103869, doi:10.1016/j.jseaes.2019.103869.

Rafie, M. T., D. P. Sahara, P. R. Cummins, W. Triyoso et al. (2023). Stress accumulation and earthquake activity on the Great Sumatran Fault, Indonesia, Nat. Hazards, 116, 3401-3425, doi:10.1007/s11069-023-05816-2.

Razin, T., M. T. Rafie, M. A. Massinai, M. A. Hamzah et al. (2023). The importance of detail fault geometry in modelling the stress changes caused by large earthquake: Case Study of 2017 Mw 6.7 Poso earthquake, IOP Conf. Ser. Earth Environ. Sci., 1288, 1, 012015, doi:10.1088/1755-1315/1288/1/012015.

Rice, J. R. and M. P. Cleary (1976). Some basic stress diffusion solutions for fluid-saturated elastic porous media with compressible constituents, Rev. Geophys., 14, 2, 227-241, doi:10.1029/RG014i002p00227.

Roeloffs, E. A. (1988). Fault instability changes induced beneath a reservoir with cyclic variations in water level, J. Geophys. Res. Solid Earth, 93, B3, 2107-2124, doi:10.1029/JB093iB03p02107.

Sgambato, C., J. P. Faure Walker, Z. K. Mildon et al. (2020). Stress loading history of earthquake faults influenced by fault/shear zone geometry and Coulomb pre-stress, Sci. Rep., 10, 1, 12724, doi:10.1038/s41598-020-69681-w.

Shikakura, Y., Y. Fukahata and K. Hirahara (2014). Long-term changes in the Coulomb failure function on inland active faults in southwest Japan due to east-west compression and interplate earthquakes, J. Geophys. Res. Solid Earth, 119, 1, 502-518, doi:10.1002/2013JB010156.

Sianipar, D., G. Daniarsyad, P. Priyobudi, N. Heryandoko et al. (2021). Rupture behaviour of the 2017 Mw 6.6 Poso earthquake in Sulawesi, Indonesia, Geod. Geodyn., 12, 5, 329-335, doi:10.1016/j.geog.2021.07.002.

Silver, E. A., R. McCaffrey and R. B. Smith (1983). Collision, rotation, and the initiation of subduction in the evolution of Sulawesi, Indonesia, J. Geophys. Res. Solid Earth, 88, B11, 9407-9418, doi:10.1029/JB088iB11p09407.

Skempton, A. W. (1954). The pore-pressure coefficients A and B, Géotechnique, 4, 4, 143-147, doi:10.1680/geot.1954.4.4.143.

Socquet, A., J. Hollingsworth, E. Pathier and M. Bouchon (2019). Evidence of supershear during the 2018 magnitude 7.5 Palu earthquake from space geodesy, Nat. Geosci., 12, 192-199, doi:10.1038/s41561-018-0296-0.

Socquet, A., W. Simons, C. Vigny, R. McCaffrey et al. (2006). Microblock rotations and fault coupling in SE Asia triple junction (Sulawesi, Indonesia) from GPS and earthquake slip vector data, J. Geophys. Res. Solid Earth, 111, B8, doi:10.1029/2005JB003963.

Song, X., Y. Zhang, X. Shan, Y. Liu et al. (2019). Geodetic observations of the 2018 Mw 7.5 Sulawesi earthquake and its implications for the kinematics of the Palu fault, Geophys. Res. Lett., 46, 4212-4220, doi:10.1029/2019GL082045.

Stein, R. S. (1999). The role of stress transfer in earthquake occurrence, Nature, 402, 605-609, doi:10.1038/45144.

Stein, R. S., A. A. Barka and J. H. Dieterich (1997). Progressive failure on the North Anatolian fault since 1939 by earthquake stress triggering, Geophys. J. Int., 128, 3, 594-604, doi:10.1111/j.1365-246X.1997.tb05321.x.

Stein, R. S., G. C. P. King and J. Lin (1994). Stress triggering of the 1994 M = 6.7 Northridge, California, earthquake by its predecessors, Science, 265, 5177, 1432-1435, doi:10.1126/science.265.5177.1432.

Stein, S. and M. Wysession (1991). An introduction to seismology, earthquakes and earth structure, Wiley-Blackwell, ISBN:978-0-865-42078-6.

Storchak, D. A., D. Di Giacomo, E. R. Engdahl, J. Harris et al. (2015). The ISC-GEM global instrumental earthquake catalogue (1900-2009): introduction, Phys. Earth Planet. Inter., 239, 48-63, doi:10.1016/j.pepi.2014.06.009.

Surmont, J., C. Laj, C. Kissel, C. Rangin et al. (1994). New paleomagnetic constraints on the Cenozoic tectonic evolution of the North Arm of Sulawesi, Indonesia, Earth Planet. Sci. Lett., 121, 3-4, 629-638, doi:10.1016/0012-821X(94)90096-5.

Toda, S., R. S. Stein, K. Richards-Dinger and S. B. Bozkurt (2005). Forecasting the evolution of seismicity in southern California: Animation built on earthquake stress transfer, J. Geophys. Res. Solid Earth, 110, B5, doi:10.1029/2004JB003415.

Toda, S., J. Lin and R. S. Stein (2011). Using the 2011 Mw 9.0 off the Pacific coast of Tohoku Earthquake to test the Coulomb stress triggering hypothesis and to calculate faults brought closer to failure, Earth Planets Space, 63, 725-730, doi:10.5047/eps.2011.05.010.

Toda, S. and R. S. Stein (2020). Long-and short-term stress interaction of the 2019 Ridgecrest sequence and Coulomb-based earthquake forecasts, Bull. Seismol. Soc. Am., 110, 4, 1765-1780, doi:10.1785/0120200169.

Tong, X., D. T. Sandwell and D. A. Schmidt (2018). Surface creep rate and moment accumulation rate along the Aceh segment of the Sumatran fault from L-band ALOS-1/PALSAR-1 observations, Geophys. Res. Lett., 45, 8, 3404-3412, doi:10.1002/2017GL076723.

U.S. Geological Survey (2018). M 7.5 −72 km N of Palu, Indonesia, https://earthquake.usgs.gov/earthquakes/eventpage/us1000h3p4/finite-fault.

Vigny, C., H. Perfettini, A. Walpersdorf, A. Lemoine et al. (2002). Migration of seismicity and earthquake interactions monitored by GPS in SE Asia triple junction: Sulawesi, Indonesia, J. Geophys. Res. Solid Earth, 107, 10, doi:10.1029/2001JB000377.

Walpersdorf, A., C. Vigny, C. Subarya and P. Manurung (1998). Monitoring of the Palu-Koro Fault (Sulawesi) by GPS, Geophys. Res. Lett., 25, 13, 2313-2316, doi:10.1029/98GL01799.

Wang, S., C. Xu, W. Xu, Z. Yin et al. (2019). The 2017 Mw 6.6 Poso Earthquake: Implications for extrusion tectonics in Central Sulawesi, Seismol. Res. Lett., 90, 2A, 649-658, doi:10.1785/0220180211.

Wessel, P., J. F. Luis, L. Uieda, R. Scharroo et al. (2019). The generic mapping tools version 6, Geochem. Geophys. Geosyst., 20, 11, 5556-5564, doi:10.1029/2019GC008515.

Zhang, Y., Y. T. Chen and W. Feng (2019). Complex multiple-segment ruptures of the 28 September 2018, Sulawesi, Indonesia, earthquake, Sci. Bull., 64, 10, 650-652, doi:10.1016/j.scib.2019.04.018.

***CORRESPONDING AUTHOR: Muhammad TAUFIQ RAFIE**,
Hasanuddin University, Department of Geophysics, Jl. Perintis Kemerdekaan No.KM.10,
Tamalanrea Indah, Kec. Tamalanrea, Kota Makassar, Sulawesi Selatan, 90245, Indonesia
e-mail: taufiqrafie@unhas.ac.id